J Nanopart Res (2024) 26:37
https://doi.org/10.1007/s11051-024-05953-0

RESEARCH PAPER

Polyol-mediated synthesis and characterization of magnesium–aluminum spinel nanoparticles

Pedro Henrique Lopes Nunes Abreu dos Santos · **Sebastião Ribeiro**

Received: 2 October 2023 / Accepted: 9 February 2024 / Published online: 17 February 2024

Abstract $MgAl_2O_4$ spinel nanoparticles were successfully synthesized using the polyol-mediated process. The study focused on the use of aluminum nitrate and magnesium acetate as precursor salts, with diethylene glycol as the solvent. The synthesis was conducted at three different temperatures: 150, 180, and 230 °C, followed by a subsequent calcination step. The dried samples consisted of a combination of magnesium oxalate and an unidentified amorphous or nanostructured phase. Upon calcination, all samples exhibited the desired $MgAl_2O_4$ spinel structure, along with a small amount of MgO. The FTIR spectra of the calcined samples confirmed the crystal structure of the $MgAl_2O_4$ phase as an inverse spinel. Scanning electron microscopy images revealed the quasi-spherical morphology of the nanoparticles, with particle sizes ranging from 70 to 120 nm for dried samples and 50 to 60 nm for calcined samples.

Keywords Magnesium–aluminum spinel · Nanoparticles · Polyol-mediated process · Synthesis · Characterization

P. H. Lopes Nunes Abreu dos Santos (✉) · S. Ribeiro
Department of Materials Engineering (DEMAR), Lorena School of Engineering (EEL), University of São Paulo (USP), Estrada Municipal Chiquito de Aquino, Nº 1000, Mondesir, Lorena, SP, Brazil
e-mail: pedroh.santos@usp.br

Introduction

Magnesium aluminate spinel (MAS) is a ceramic material with a wide range of applications due to its excellent properties, such as high melting temperature (2135 °C), low density (3.58 $g \times cm^{-1}$), high hardness (16 GPa), high mechanical strength (135–216 MPa at room temperature and 120–205 MPa at 1300 °C), low coefficient of thermal expansion (9×10^{-6} $°C^{-1}$ between 30 and 1400 °C), as well as high mechanical resistance, high chemical attack resistance, high thermal shock resistance, and a wide energy band gap [1]. Therefore, MAS can be applied as a refractory material [2–4], transparent ceramics [5–7], catalyst support [8–10], or active phase of photocatalysts [11, 12], an active component of sensors [13, 14] among other applications.

The crystal structure of this oxide is face-centered cubic, and it belongs to the Fd-3 m space group. The divalent cations Mg^{2+} are positioned similarly to carbon in a diamond crystal and form tetrahedral sites concerning oxygen atoms, while the trivalent cations Al^{3+} form octahedral sites concerning oxygen atoms [1]. There is also the possibility that the trivalent cations partially or completely occupy tetrahedral sites, leading to the divalent cations occupying the remaining octahedral sites. In this context, this oxide is referred to as an inverse spinel [15].

MAS is rarely found in nature. Therefore, it needs to be synthesized. Synthesis methods for spinel can be mainly divided into two categories: solid-state

reactions and wet-chemical reactions. Despite enabling the production of a large volume of MAS, which is required, for instance, when the oxide is applied as a refractory material, synthesis from solid-state reactions requires high temperatures (up to 1600 °C), which significantly increases the cost of the final product. Another significant drawback of this synthesis method is the inability to control the textural properties or the shape of crystals [1].

Among the wet-chemical reaction methods, some are well-documented in the literature. The sol–gel process typically uses alkoxides as precursors for Mg^{2+} and Al^{3+} cations. Reactions are performed at low temperatures (< 100 °C), and thermal treatment in the range of 700 to 1000 °C to achieve the formation of spinel with a well-defined crystalline structure, uniform particle size distribution, and usually in the nanoscale [16–20]. The synthesis of MAS through the co-precipitation process also maintains low reaction temperatures, depending on a thermal treatment similar to those required in the sol–gel process, and it employs reagents that are slightly less expensive than those used in the sol–gel process [21–25]. Flame spray pyrolysis is another viable option for synthesis when precise control of the final properties of spinel is crucial [26, 27]. Another widely described option in the literature is the combustion synthesis method [28, 29].

Despite being crucial for the development of materials with increasingly well-defined characteristics, wet-chemical reaction methods still have some limitations. The sol–gel synthesis of MAS, for instance, involves the use of relatively costly reagents. In the context of the co-precipitation process, there is a significant tendency for particle agglomeration coupled with reduced sinterability, similar to oxides prepared through flame spray pyrolysis. In the case of combustion synthesis, the final material may contain a high degree of impurities, which can considerably influence its properties and restrict the potential applications of the spine [30].

An analysis of the synthesis methods outlined in the literature exposes gaps in the advancement of this pivotal material, whether in the pursuit of enhanced physicochemical properties, scale-up of production, or the implementation of more cost-effective and efficient synthesis methodologies.

In this context, this study presents a novel alternative synthesis method for magnesium–aluminum spinel. The synthesis of this oxide via the polyol-mediated process, which has not been extensively investigated in the pertinent literature, will be exhaustively elucidated herein to broaden the spectrum of available methods for synthesizing this material.

Polyol-mediated process for nanoparticle synthesis

The polyol-mediated process entails the synthesis of particles, typically at a nanoscale, from organic or inorganic salts dissolved in a polyol. Polyols refer to polyhydric alcohols, such as ethylene glycol and propylene glycol, or ether glycols like diethylene glycol, triethylene glycol, or tetraethylene glycol [31]. This method was initially developed by Fiévet et al. [32] for the synthesis of metallic nanoparticles and was subsequently extended to the synthesis of oxides by Jézéquel et al. [33]. The polyol-mediated synthesis is closely linked to a parameter known as the hydrolysis ratio (h), which represents the ratio of water molecules in the system to the metal ions in solution. It is noteworthy that at very high hydrolysis ratio values, a preference for the formation of hydroxides over oxides is observed.

Some properties of polyols are integral to their suitability for use in this synthesis method. Firstly, most water-soluble salts are also soluble in polyols. Secondly, the boiling points of polyols generally fall within the range of 200 to 300 °C, obviating the necessity for pressurized systems to achieve the high crystallinity of particles typically required in solvothermal treatments. Furthermore, in addition to the aforementioned properties, polyols also demonstrate chelating agent characteristics, which facilitate the synthesis of finely sized particles within a well-defined range, thereby preventing their agglomeration [34].

This study has the objective of proposing a viable route to synthesize $MgAl_2O_4$ spinel using the polyol-mediated process, with aluminum nitrate and magnesium acetate as precursor salts and diethylene glycol as the polyol solvent.

Materials and methods

Synthesis

The preparation of nanoscale magnesium–aluminum spinel (MAS) particles involved the mixing of $Mg(CH_3COO)_2{\cdot}4H_2O$ and $Al(NO_3)_3{\cdot}9H_2O$

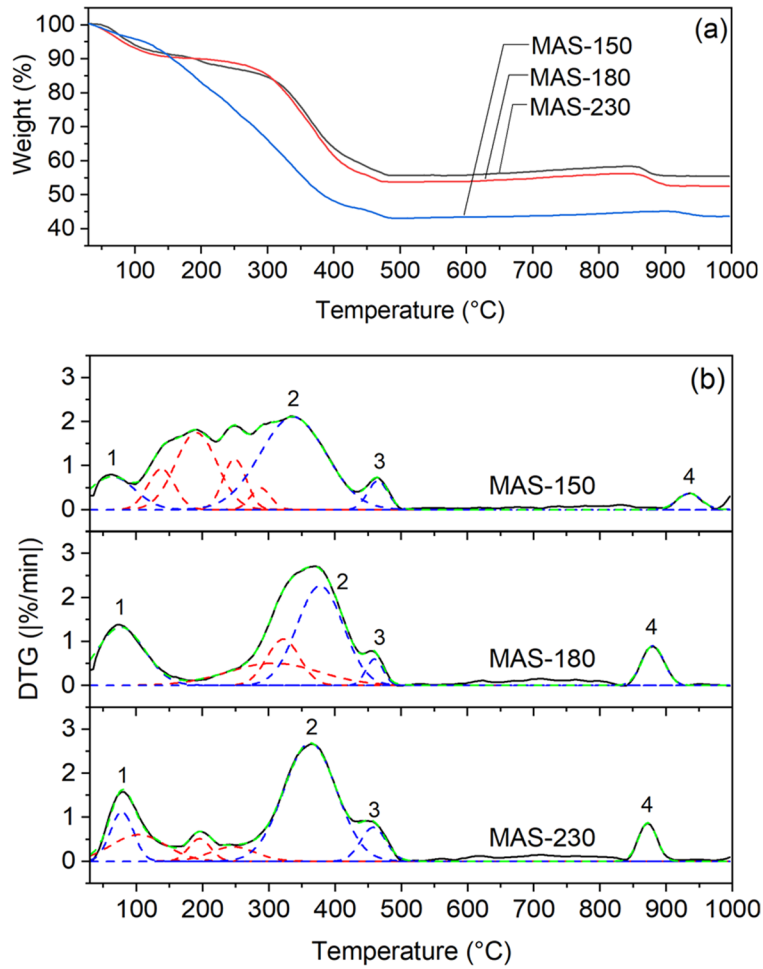

Fig. 1 **a** Thermogravimetry profile for MAS-150, MAS-180, and MAS-230 and **b** DTG modulus for MAS-150, MAS-180, and MAS-230

Table 1 Mass loss of uncalcined samples obtained by TGA up to 1000° C

Sample	Mass loss (%)
MAS-150	56.32
MAS-180	47.45
MAS-230	44.58

to maintain an Al/Mg molar ratio of 2, resulting in the production of 5 g of MAS. Notably, the precursor salts already contained some water molecules within their structures, eliminating the need for additional water to achieve a hydrolysis ratio greater than zero. Subsequently, the precursor salts were combined with 200 g of diethylene glycol (DEG). The resulting mixture was heated in an open system until reaching the desired temperature. A condenser was then connected to the system to prevent the evaporation of the liquid phase and maintain the temperature for 2 h. Three distinct temperatures were utilized: 150, 180, and 230 °C. The synthesized materials underwent subsequent washing with ethanol, followed by drying at 80 °C for 2 h and categorization into MAS-150, MAS-180, and MAS-230 based on the synthesis temperature. After characterizing the dried materials, they were subjected to calcination at 800 °C for 2 h and designated as MAS-150-C, MAS-180-C, and MAS-230-C, respectively, based on the synthesis temperature.

Characterization

The dried samples underwent characterization through thermogravimetry (TG), X-ray diffractometry (XRD), Fourier-transform infrared spectrometry (FTIR), and scanning electron microscopy with a field-emission gun

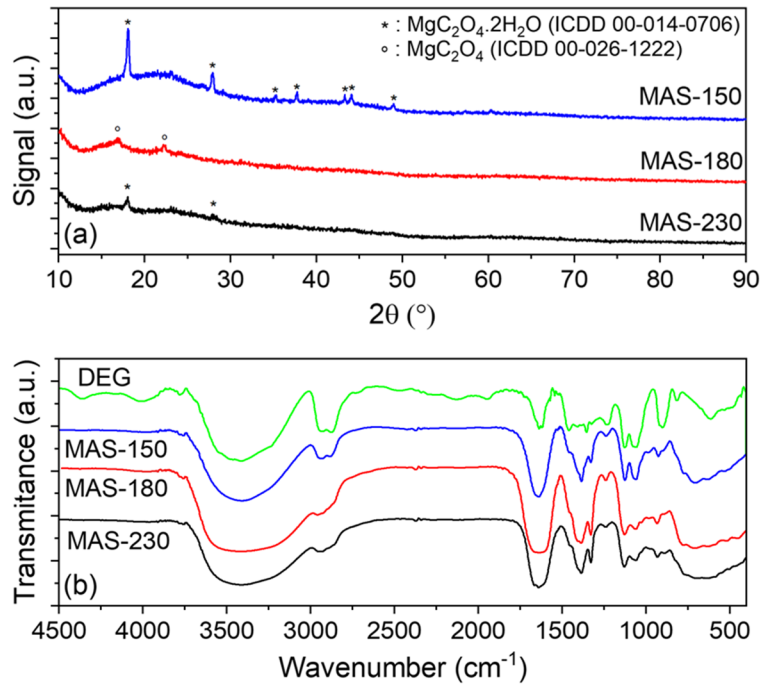

Fig. 2 **a** XRD of dried samples and **b** FTIR of dried samples compared to DEG

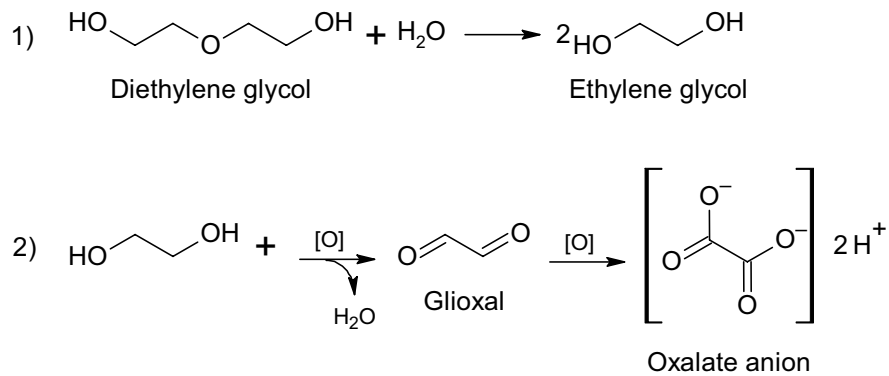

Fig. 3 Formation of oxalate anion from DEG decomposition

(FE-SEM). Subsequently, the calcined samples were characterized using XRD, FTIR, and FE-SEM.

Thermogravimetric (TG) analysis was conducted using a NETZSCH STA 449 F3 thermobalance with a heating rate of 5 °C/min up to 1000 °C. X-ray diffractometry (XRD) analysis was performed on a PANalytical Empyrean diffractometer employing Cu-kα radiation within the range of $10° < 2\theta < 90°$. Fourier-transform infrared spectrometry (FTIR) analysis was carried out using a Shimazu IRPrestige-21 spectrometer, covering the wavenumber range from 4000 to 450 cm^{-1}. Field-emission scanning electron microscopy (FE-SEM) analysis was conducted utilizing a Tescan Mira-4 microscope.

Results and discussion

Thermogravimetry

The thermogravimetric curves (Fig. 1a) exhibit distinct thermal decomposition profiles for three materials. Notably, the total mass variation after the analysis directly correlates with the synthesis temperature, a relationship detailed in Table 1. Further insights into these differences are provided by the derivative thermogravimetric (DTG) curves (Fig. 1b), which reveal comparable thermal events denoted by the numbers 1, 2, 3, and 4. These events correspond to the evaporation of adsorbed water from the sample surface (event

Table 2 Assignment of FTIR spectra for MAS-150, MAS-180, MAS-230, and DEG. Band positions in wavenumber (cm^{-1})

MAS-150	MAS-180	MAS-230	DEG	Assignment
3416	3416	3416	3416	OH stretch
2940	2956	2956	2956	CH_2 antisym. stretch
2874	2857	2857	2857	CH_2 sym. stretch
1642	1642	1642	-	Carboxyl salt – CO_2
			1642	OH bending
1462	1462	1462	1462	CH_2 bending
1396	1396	1396	-	Carboxyl salt – CO_2
1330	1330	1330	1330	CH_2 wagging
1248	1248	1248	1248	COC stretch
1133	1133	1133	1133	C–O stretch
1068	1051	1051	1051	C–O stretch
920	920	920	920	COH stretch

1), the thermal decomposition of the predominant material phase (events 2 and 3), and the alteration in the crystalline structure leading to the formation of the spinel phase (event 4).

In addition to the previously mentioned thermal events, it is noteworthy that additional chemical reactions take place within the temperature range of 100 to 300 °C, resulting in distinct DTG profiles for the three samples within this temperature range. Specifically, the MAS-150 sample exhibits the highest number of thermal reactions in this range, leading to a greater mass variation compared to the MAS-180 and MAS-230 samples, as depicted in Fig. 1a. This behavior can be attributed to the insufficient temperature to fully decompose the precursor salts during synthesis. Consequently, various organic complexes derived from the aluminum and magnesium cations in the solution may form, along with the potential presence of an excess of precursor salts. These factors likely contribute to the greater mass variation observed in the MAS-150 sample compared to the other two samples.

Table 3 Molar fraction of identified crystal phases in calcined samples

Sample	$MgAl_2O_4$ (%)	MgO (%)
MAS-150-C	93.6	6.4
MAS-180-C	97.7	2.3
MAS-230-C	97.8	2.2

XRD and FTIR of dried samples

The X-ray diffractograms of the dried samples (Fig. 2a) reveal the presence of magnesium oxalate

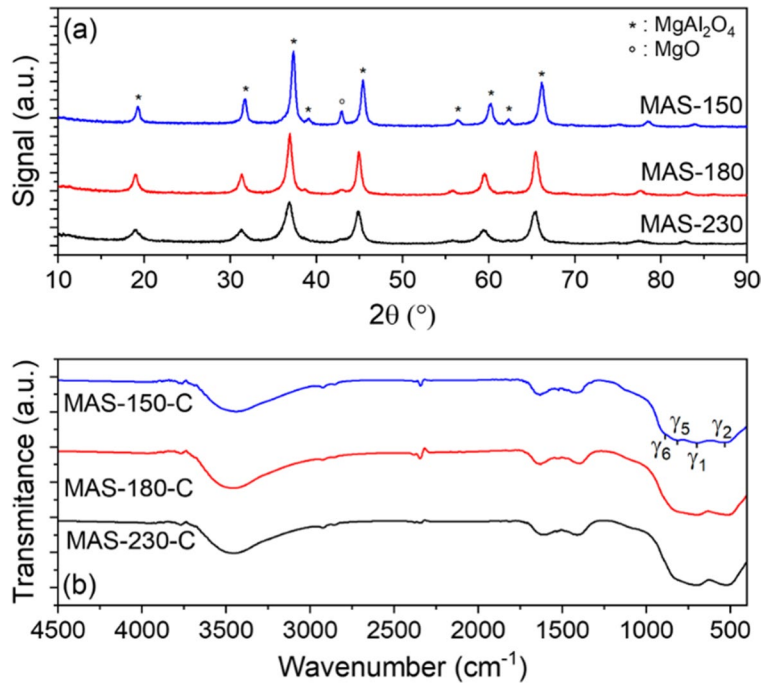

Fig. 4 **a** XRD of calcined samples and **b** FTIR of calcined samples

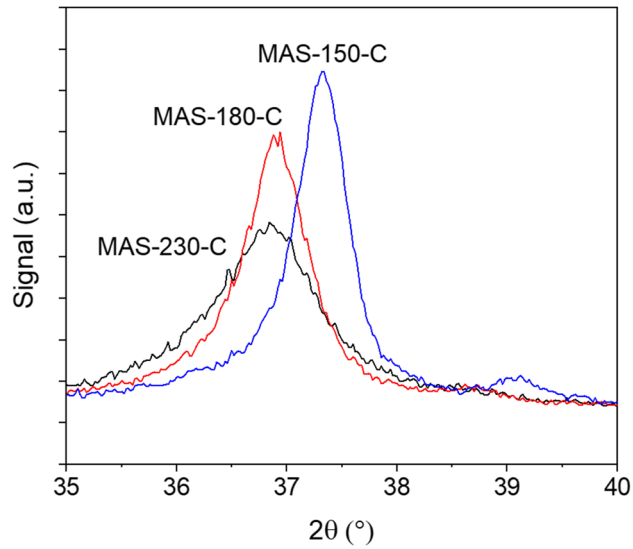

Fig. 5 Peak displacement in plane (1 1 3) of calcined samples

Table 4 Cell parameters of $MgAl_2O_4$ observed in calcined samples calculated by Rietveld refinement

Sample	MAS cell parameters *a*, *b,* and *c* (Å)
MAS-150-C	7.994
MAS-180-C	8.068
MAS-230-C	8.093

Table 5 Crystallite size calcined samples calculated by Scherrer equation

Sample	MAS crystallite size (nm)	Standard deviation (nm)
MAS-150-C	11.1	1.5
MAS-180-C	10.2	0.1
MAS-230-C	6.7	0.3

dihydrate in MAS-150 and MAS-230, while magnesium oxalate anhydrous is observed in MAS-180. The formation of the oxalate anion can be attributed to a two-step decomposition sequence in the polyol (depicted in Fig. 3) as follows:

1. The hydrolysis of the ether function of diethylene glycol
2. The complete oxidation of ethylene glycol formed through the initial reaction

The low intensity of the peaks corresponding to both types of salts suggests that only a small fraction of magnesium exists in the form of an oxalate salt. Furthermore, broad peaks present in each sample indicate the presence of a proportion of the material with an amorphous or nanostructured morphology. This phase likely encompasses Al^{3+} and the remaining Mg^{2+} cations.

The FTIR spectra of all three samples (Fig. 2b) display similar bands, suggesting a high degree of similarity among the materials. The observed bands at 3416, 2940, 2874, 1642, 1462, 1330, 1248, 1133, 1051, and 920 cm^{-1} are also apparent in the diethylene glycol (DEG) spectrum [35], indicating that some DEG remains adsorbed on the material's surface. The presence of a carboxyl salt is confirmed by the bands at 1642 cm^{-1} and 1396 cm^{-1}, indicative of the presence of magnesium acetate in all samples. This information is summarized in Table 2.

XRD and FTIR of calcined samples

The X-ray diffractograms of the calcined samples (Fig. 4a) reveal the presence of $MgAl_2O_4$ spinel and a small quantity of MgO in all the materials. Table 3 presents the estimated molar fraction of MgO, calculated using the Rietveld refinement method. These findings suggest that the $MgAl_2O_4$ structure may form due to the thermal decomposition of the amorphous phase detected in the dried materials. Alternatively, the MgO structure could arise from the thermal decomposition of magnesium oxalate present in the dried materials.

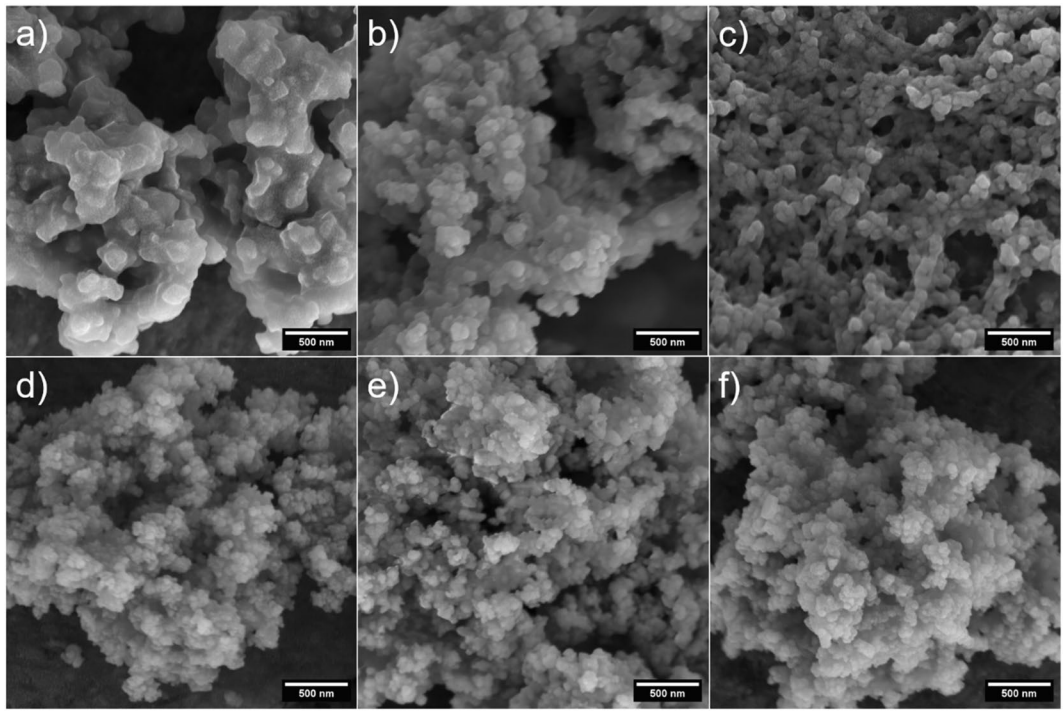

Fig. 6 FE-SEM micrographs of samples **a** MAS-150, **b** MAS-180, **c** MAS-230, **d** MAS-150-C, **e** MAS-180-C, and **f** MAS-230-C. Scale bar, 500 nm

Table 6 MAS particle size according to FE-SEM measurements

Dried sample	Particle diameter (nm)	Calcined sample	Particle diameter (nm)
MAS-150	118 (±40)	MAS-150 C	52 (±13)
MAS-180	70 (±17)	MAS-180 C	56 (±14)
MAS-230	72 (±19)	MAS-230 C	57 (±13)

An additional noteworthy observation is the displacement of peaks in MAS-150-C compared to MAS-180-C and MAS-230-C. Figure 5 illustrates this displacement for the crystallographic plane (1 1 3), resulting in a slight difference between the cell parameters of MAS-150-C and the other two calcined samples. Table 4 presents the calculated cell parameters for all three materials using the Rietveld refinement method. Figure 5 also depicts a variance in peak width, indicating differences in crystallite size. Table 4 provides the estimated crystallite sizes for all samples, calculated using the Scherrer equation.

A plausible explanation for the observed peak shift in MAS-150-C could be the higher concentration of MgO in this sample, as indicated in Table 3. The presence of a greater amount of this segregated oxide implies an excess of Al^{3+} cations in the spinel structure, resulting in a non-stoichiometric oxide. Since the ionic radius of Al^{3+} (67.5 pm) is smaller than that of Mg^{2+} (86 pm), an increased quantity of Al^{3+} ions replacing the tetrahedral sites originally occupied by Mg^{2+} ions would lead to a reduction in the unit cell volume of the spinel. Consequently, this reduction would cause a decrease in the lattice parameters *A*, *B*, and *C*, and thus a shift of the observed peaks in XRD toward higher 2θ angles. This hypothesis finds support in the work of Shou-Yong [36], who experimentally and theoretically demonstrated that non-stoichiometric spinels with higher Al^{3+} cation content indeed possess a smaller unit cell volume.

The data presented in Tables 3, 4 and 5 suggest that the molar fraction of $MgAl_2O_4$ and MgO, the cell parameters of $MgAl_2O_4$, and the crystallite size may be influenced by the synthesis temperature. Specifically, higher temperatures appear to result in an increased molar fraction of $MgAl_2O_4$, slightly larger cell parameter values, and smaller crystallites.

The FTIR spectra of the calcined samples (Fig. 4a) provide further insights into the structure of $MgAl_2O_4$ spinel. All samples exhibit characteristic bands: γ_6 at 900 cm^{-1}, γ_5 at 815 cm^{-1}, γ_1 at 700 cm^{-1}, and γ_2 at 520 cm^{-1}. According to Erukhimovitch et al. [37], γ_1 and γ_2 correspond to the vibration of trivalent cations (Al^{3+}) in octahedral sites, while the presence of γ_5 and γ_6 indicates that a portion of Al^{3+} also occupies tetrahedral voids. The presence of all these bands indicates that $MgAl_2O_4$ is a partially inverted spinel in all of the samples.

FE-SEM

The FE-SEM micrographs (Fig. 6a, b, and c) reveal that the morphology of the dried samples exhibits no significant differences. All samples consist of nearly spherical particles with a uniform distribution of diameters. The measurement of the particle diameters (Table 6) reveals that low synthesis temperature influences the size of the particles in merely dried samples since MAS-150 presents larger particles than MAS-180 and MAS-230. In calcined samples (Fig. 6d, e and f), analyzing Table 6, it is possible to note that the nanoparticles present the same size in all the samples. These results corroborate what was observed in the thermogravimetric analyses, as it is expected for samples that present a higher mass loss, that also present a greater variation in calcination.

Conclusions

MAS nanoparticles were successfully synthesized by the polyol-mediated process. Characterization of the samples before the calcination step (mainly TG and FTIR analyses) shows that immediately after synthesis, the material appears to be composed of a set of non-identified complexes formed with Mg^{2+} and Al^{3+} ions, and the nature of these complexes strongly depends on the temperature adopted during the synthesis step.

After calcination, XRD and FTIR analyses confirm the conversion of these complexes into magnesium–aluminum spinel with small amounts of excess magnesium oxide. A more detailed analysis of the FTIR results reveals that the spinel structure has characteristics of a non-stoichiometric material. FE-SEM results show that there are no major differences in the morphology of the final materials according to the adopted synthesis temperatures. After calcination all samples have similar size, approximately 50 nm.

Funding This research has received support from the Coordenação de Aperfeiçoamento de Pessoal de Nível Superior—Brasil (CAPES)—finance code 88887.464399/2019–00 and the Conselho Nacional de Desenvolvimento Científico e Tecnológico—Brasil (CNPq)—finance code 313915/2021–0.

Declarations

Conflict of interest The authors declare no competing interests.

References

1. Ganesh I (2013) A review on magnesium aluminate (MgAl2O4) spinel: synthesis, processing and applications. Int Mater Rev 58(2):63–112. https://doi.org/10.1179/1743280412Y.0000000001
2. Lv L, Xiao G, Ding D (2021) Improved thermal shock resistance of low-carbon Al2O3–C refractories fabricated with C/MgAl2O4 composite powders. Ceram Int 47(14):20169–20177. https://doi.org/10.1016/J.CERAMINT.2021.04.023
3. Shafiee H, Salehirad A, Samimi A (2020) Effect of synthesis method on structural and physical properties of MgO/MgAl2O4 nanocomposite as a refractory ceramic. Appl Phys A Mater Sci Process 126(3). https://doi.org/10.1007/s00339-020-3369-z
4. Gu Q, Zhao F, Liu X, Jia Q (2019) Preparation and thermal shock behavior of nanoscale MgAl2O4 spinel-toughened MgO-based refractory aggregates. Ceram Int 45(9):12093–12100. https://doi.org/10.1016/J.CERAMINT.2019.03.107
5. Gajdowski C et al (2017) Influence of post-HIP temperature on microstructural and optical properties of pure MgAl2O4 spinel: from opaque to transparent ceramics. J Eur Ceram Soc 37(16):5347–5351. https://doi.org/10.1016/J.JEURCERAMSOC.2017.07.031
6. Balabanov SS et al (2015) Fabrication of transparent MgAl2O4 ceramics by hot-pressing of sol-gel-derived nanopowders. Ceram Int 41(10):13366–13371. https://doi.org/10.1016/J.CERAMINT.2015.07.123
7. Zhang P et al (2015) Aqueous gelcasting of the transparent MgAl2O4 spinel ceramics. J Alloys Compd 646:833–836. https://doi.org/10.1016/J.JALLCOM.2015.05.275
8. Yu S, Hu Y, Cui H, Cheng Z, Zhou Z (2021) Ni-based catalysts supported on MgAl2O4 with different properties for combined steam and CO2 reforming of methane. Chem Eng Sci 232:116379. https://doi.org/10.1016/J.CES.2020.116379
9. Rezaei M, Alavi SM (2019) Dry reforming over mesoporous nanocrystalline 5% Ni/M-MgAl2O4 (M: CeO2, ZrO2, La2O3) catalysts. Int J Hydrogen Energy 44(31):16516–16525. https://doi.org/10.1016/J.IJHYDENE.2019.04.213
10. Qiu Y, Fu E, Gong F, Xiao R (2022) Catalyst support effect on ammonia decomposition over Ni/MgAl2O4 towards hydrogen production. Int J Hydrogen Energy 47(8):5044–5052. https://doi.org/10.1016/J.IJHYDENE.2021.11.117
11. Wongtawee W, Amornpitoksuk P, Randorn C, Rattana T, Suwanboon S (2022) Photocatalytic activity under visible light illumination of organic dyes over g-C3N4/MgAl2O4

nanocomposite. J Indian Chem Soc 99(8):100628. https://doi.org/10.1016/J.JICS.2022.100628
12. Wongtawee W, Amornpitoksuk P, Randorn C, Rattana T, Suwanboon S (2023) Amelioration of photocatalytic activity of MgAl2O4 spinel photocatalyst by coupling with WO3. Inorg Chem Commun 152:110654. https://doi.org/10.1016/J.INOCHE.2023.110654
13. Riahi R, Taher MA, Beitollahi H (2022) Hydroxylamine electrochemical sensor based on magnesium aluminate spinel nanoparticles modified electrode. Int J Environ Anal Chem 1–13. https://doi.org/10.1080/03067319.2022.2118587
14. Li X et al (2022) Insight into site occupancy of cerium and manganese ions in MgAl2O4 and their energy transfer for dual-mode optical thermometry. J Alloys Compd 928:166701. https://doi.org/10.1016/J.JALLCOM.2022.166701
15. Hatton P, Uberuaga BP (2023) Short range order in disordered spinels and the impact on cation vacancy transport. J Mater Chem A Mater 11(7):3471–3480. https://doi.org/10.1039/D2TA06102C
16. Lepkova D, Batarjav A, Samuneva B, Ivanova LGY (1991) Preparation and properties of ceramics from magnesium spinel by sol-gel technology. J Mater Sci 26(4861):4864
17. Yuan Y, Zhang S, You W (2004) Synthesis of MgAl2O4 spinel nanometer powder via biology polysaccharide assisted sol-gel process. J Solgel Sci Technol 30:223–227
18. Sanjabi S, Obeydavi A (2015) Synthesis and characterization of nanocrystalline MgAl2O4 spinel via modified sol–gel method. J Alloys Compd 645:535–540. https://doi.org/10.1016/j.jallcom.2015.05.107
19. Zarazúa-Villalobos L, Téllez-Jurado L, Vargas-Becerril N, Fantozzi G, Balmori-Ramírez H (2015) Synthesis of magnesium aluminate spinel nanopowder by sol–gel and low-temperature processing. J Solgel Sci Technol 85(1):110–120. https://doi.org/10.1007/s10971-017-4526-5
20. Khomidov FG, Kadyrova ZR, Usmanov KhL, Niyazova ShM, Sabirov BT (2021) Peculiarities of sol-gel synthesis of aluminum-magnesium spinel. Glass Ceram 78(5–6):251–254. https://doi.org/10.1007/s10717-021-00389-7
21. Li J-G, Ikegami T, Lee J-H, Mori T, Yajima Y (2001) A wet-chemical process yielding reactive magnesium aluminate spinel (MgAl2O4) powder. Ceram Int 27(4):481–489. https://doi.org/10.1016/S0272-8842(00)00107-3
22. Zawrah MF, Hamaad H, Meky S (2007) Synthesis and characterization of nano MgAl2O4 spinel by the co-precipitated method. Ceram Int 33(6):969–978. https://doi.org/10.1016/j.ceramint.2006.02.015
23. Wajler A, Tomaszewski H, Drożdż-Cieśla E, Węglarz H, Kaszkur Z (2008) Study of magnesium aluminate spinel formation from carbonate precursors. J Eur Ceram Soc 28(13):2495–2500. https://doi.org/10.1016/j.jeurceramsoc.2008.03.013
24. Rashad MM, Zaki ZI, El-Shall H (2009) A novel approach for synthesis of nanocrystalline MgAl2O4 powders by co-precipitation method. J Mater Sci 44(11):2992–2998. https://doi.org/10.1007/s10853-009-3397-8
25. Rufner J, Anderson D, van Benthem K, Castro RHR (2013) Synthesis and sintering behavior of ultrafine (<10 nm) magnesium aluminate spinel nanoparticles. J Am Ceram Soc 96(7):2077–2085. https://doi.org/10.1111/jace.12342
26. Suyama Y, Kato A (1982) Characterization and sintering of Mg Al spinel prepared by spray-pyrolysis technique. Ceram Int 8(1):17–21. https://doi.org/10.1016/0272-8842(82)90010-4
27. Bickmore CR, Waldner KF, Treadwell DR, Laine RM (1996) Ultrafine spinel powders by flame spray pyrolysis of a magnesium aluminum double alkoxide. J Am Ceram Soc 79(5):1419–1423. https://doi.org/10.1111/j.1151-2916.1996.tb08608.x
28. Tong Y, Zhao S, Ma L, Zhao W, Song W, Yang H (2013) Facile synthesis and crystal growth dynamics study of MgAl2O4 nanocrystals. Mater Res Bull 48(11):4834–4838. https://doi.org/10.1016/j.materresbull.2013.08.039
29. Sarkar R, Das S (2014) Auto combustion synthesis for magnesium aluminate spinel using glycine as fuel and its sintering study. Trans Indian Ceram Soc 73(2):172–176. https://doi.org/10.1080/0371750X.2014.922436
30. Baruah B, Bhattacharyya S, Sarkar R (2023) Synthesis of magnesium aluminate spinel—an overview. Int J Appl Ceram Technol 20(3):1331–1349. https://doi.org/10.1111/ijac.14309
31. Fiévet F, Brayner R (2013) "The polyol process", in Nanomaterials: a danger or a promise? London Springer, London 1:25. https://doi.org/10.1007/978-1-4471-4213-3_1
32. Fievet F, Lagier JP, Blin B, Beaudoin B, Figlarz M (1989) Homogeneous and heterogeneous nucleations in the polyol process for the preparation of micron and submicron size metal particles. Solid State Ion 32–33(PART 1):198–205. https://doi.org/10.1016/0167-2738(89)90222-1
33. Jézéquel D, Guenot J, Jouini N, Fiévet F (1995) Submicrometer zinc oxide particles: elaboration in polyol medium and morphological characteristics. J Mater Res 10(1):77–83. https://doi.org/10.1557/JMR.1995.0077
34. Fiévet F et al (2018) The polyol process: a unique method for easy access to metal nanoparticles with tailored sizes, shapes and compositions. Chem Soc Rev 47(14):5187–5233. https://doi.org/10.1039/C7CS00777A
35. Ahmed KM, McLeod MP, Nézivar J, Giuliani AW (2010) Fourier transform infrared and near-infrared spectroscopic methods for the detection of toxic diethylene glycol (DEG) contaminant in glycerin based cough syrup. Spectroscopy 24(6):601–608. https://doi.org/10.3233/SPE-2010-0482
36. Shou-Yong J, Li-Bin L, Ning-Kang H, Jin Z, Yong L (2000) Investigation on lattice constants of Mg-Al spinels. J Mater Sci Lett 19(3):225–227. https://doi.org/10.1023/A:1006710808718
37. Erukhimovitch V, Mordekoviz Y, Hayun S (2015) Spectroscopic study of ordering in non-stoichiometric magnesium aluminate spinel. Am Miner 100(8–9):1744–1751. https://doi.org/10.2138/am-2015-5266